In-flight observations of low-mode #R asymmetries in NIF implosions

PSFC/JA-14-3

In-flight observations of low-mode ρR asymmetries in NIF implosions

A. B. Zylstra,[1, *] J. A. Frenje,[1] F. H. S´eguin,[1] J. R. Rygg,[2] A. Kritcher,[2] M. J. Rosenberg,[1] H. G. Rinderknecht,[1] D. G. Hicks,[2] S. Friedrich,[2] R. Bionta,[2] R. Olson,[3, 4] J. Atherton,[2] M. Barrios,[2] P. Bell,[2] R. Benedetti,[2] L. Berzak Hopkins,[2] R. Betti,[5] D. Bradley,[2] D. Callahan,[2] D. Casey,[2] G. Collins,[2] E. L. Dewald,[2] S. Dixit,[2] T. Döppner,[2] M. J. Edwards,[2] M. Gatu Johnson,[1] S. Glenn,[2] G. Grim,[4] S. Hatchett,[2] O. Jones,[2] S. Khan,[2] J. Kilkenny,[6] J. Kline,[4] J. Knauer,[5] G. Kyrala,[4] O. Landen,[2] S. LePape,[2] C. K. Li,[1] J. Lindl,[2] T. Ma,[2] A. Mackinnon,[2] M. J.-E. Manuel,[1] N. B. Meezan,[2] D. Meyerhofer,[5] E. Moses,[2] S. Nagel,[2] A. Nikroo,[6] T. Parham,[2] A. Pak,[2] R. D. Petrasso,[1] R. Prasad,[2] J. Ralph,[2] H. F. Robey,[2] J. S. Ross,[2] T. C. Sangster,[5] S. Sepke,[2] N. Sinenian,[1] H. W. Sio,[1] B. Spears,[2] R. Tommasini,[2] R. Town,[2] S. Weber,[2] D. Wilson,[4] C. Yeamans,[2] and R. Zacharias[2]

1: Plasma Science and Fusion Center, MIT
2: Lawrence Livermore National Laboratory
3: Sandia National Laboratory
4: Los Alamos National Laboratory
5: Laboratory for Laser Energetics
6: General Atomics

March, 2014

Plasma Science and Fusion Center
Massachusetts Institute of Technology
Cambridge MA 02139 USA

This work was supported by by the U.S. DoE (Grant No. DE-NA0001857, DE-FC52-08NA28752), LLNL (No. B597367), LLE (No. 415935- G), the Fusion Science Cen- ter at the University of Rochester (No. 524431), and the National Laser Users Facility (No. DE-NA0002035). This material is based upon work supported by the Na- tional Science Foundation Graduate Research Fellowship Program under Grant No. 1122374.

Draft March 7, 2014

In-flight observations of low-mode ρR asymmetries in NIF implosions

A. B. Zylstra,[1,*] J. A. Frenje,[1] F. H. Séguin,[1] J. R. Rygg,[2] A. Kritcher,[2] M. J. Rosenberg,[1] H. G. Rinderknecht,[1] D. G. Hicks,[2] S. Friedrich,[2] R. Bionta,[2] R. Olson,[3,4] J. Atherton,[2] M. Barrios,[2] P. Bell,[2] R. Benedetti,[2] L. Berzak Hopkins,[2] R. Betti,[5] D. Bradley,[2] D. Callahan,[2] D. Casey,[2] G. Collins,[2] E. L. Dewald,[2] S. Dixit,[2] T. Döppner,[2] M. J. Edwards,[2] M. Gatu Johnson,[1] S. Glenn,[2] G. Grim,[4] S. Hatchett,[2] O. Jones,[2] S. Khan,[2] J. Kilkenny,[6] J. Kline,[4] J. Knauer,[5] G. Kyrala,[4] O. Landen,[2] S. LePape,[2] C. K. Li,[1] J. Lindl,[2] T. Ma,[2] A. Mackinnon,[2] M. J.-E. Manuel,[1] N. B. Meezan,[2] D. Meyerhofer,[5] E. Moses,[2] S. Nagel,[2] A. Nikroo,[6] T. Parham,[2] A. Pak,[2] R. D. Petrasso,[1] R. Prasad,[2] J. Ralph,[2] H. F. Robey,[2] J. S. Ross,[2] T. C. Sangster,[5] S. Sepke,[2] N. Sinenian,[1] H. W. Sio,[1] B. Spears,[2] R. Tommasini,[2] R. Town,[2] S. Weber,[2] D. Wilson,[4] C. Yeamans,[2] and R. Zacharias[2]

[1] *Plasma Science and Fusion Center, Massachusetts Institute of Technology, Cambridge, MA 02139, USA*
[2] *Lawrence Livermore National Laboratory, Livermore, CA 94550, USA*
[3] *Sandia National Laboratory, Albuquerque, NM 87185, USA*
[4] *Los Alamos National Laboratory, Los Alamos, NM 87545, USA*
[5] *Laboratory for Laser Energetics, University of Rochester, Rochester, NY 14623, USA*
[6] *General Atomics, San Diego, CA 92186, USA*

(Dated: March 7, 2014)

Charged-particle spectroscopy is used to assess implosion symmetry in ignition-scale indirect-drive implosions for the first time. Surrogate D^{3}He gas-filled implosions at the National Ignition Facility produce energetic protons via D+^{3}He fusion that are used to measure the implosion areal density (ρR) at the shock-bang time. By using protons produced several hundred ps before the main compression bang, the implosion is diagnosed in-flight at a convergence ratio of 3-5 just prior to peak velocity. This isolates acceleration-phase asymmetry growth. For many surrogate implosions, proton spectrometers placed at the north pole and equator reveal significant asymmetries with amplitudes routinely $\gtrsim 10\%$. With significant expected growth by stagnation, it is likely that these asymmetries would degrade the final implosion performance. X-ray self-emission images at stagnation appear more symmetric than expected, suggesting the hot-spot shape does not reflect the stagnated shell shape, as seen in recent computational studies [R.H.H. Scott et al., Phys. Rev. Let.. 110, 075001 (2013)].

The central challenge of Inertial Confinement Fusion (ICF) is to compress and heat fusion fuel to the extreme conditions required for ignition and burn [1, 2]. At the National Ignition Facility (NIF) [3], the approach to achieving this is by symmetric, ablatively-driven spherical compression, where the goal is a convergence ratio $CR \equiv R_{initial}/R_{final} \sim 35$. Ignition experiments must control the cold-fuel symmetry to better than several percent at stagnation[2, 4, 5]. In indirect-drive implosions conducted at the NIF, radiation drive non-uniformities can cause detrimental low-mode ($\lesssim 8$) asymmetries[6, 7], the focus of this work.

Several techniques are used to study asymmetry at the NIF; in this Letter we present the first charged-particle measurements of areal-density (ρR) asymmetries at shock-bang time in ignition-scale implosions. These measurements are novel in quantifying ρR asymmetries that are present when the implosion is in-flight, at $CR \sim 3-5$, complementing prior methods at different CR. It is directly comparable to recently-developed in-flight radiography of the imploding shell[8], which can be used simultaneously with the charged-particle diagnostics. Other techniques for diagnosing symmetry include 'Re-Emit' experiments that measure x-ray re-emission from a high-Z capsule to diagnose early-time ($CR \sim 1$) hohlraum drive asymmetries[9, 10] and shock-timing experiments that use multiple views to diagnose early-time shock symmetry[11, 12]. In addition, x-ray self-emission produced by the implosion at stagnation is imaged to diagnose the final hot-spot symmetry in lower-convergence ($CR \sim 15-20$) surrogate implosions [13]. Finally, in cryogenic implosions, the final stagnated hot-spot and cold-fuel shapes are diagnosed by x-ray[14] and neutron[15] techniques.

Charged-particle measurements of ρR asymmetries have previously been used at the OMEGA laser facility[16] for spherically symmetric direct-drive implosions [17] and direct-drive implosions with induced asymmetries[18]. Extending this technique to NIF has been discussed[19]. The reaction

$$\mathrm{D} + {}^3\mathrm{He} \rightarrow {}^4\mathrm{He}\ (3.6\ \mathrm{MeV}) + \mathrm{p}\ (14.7\ \mathrm{MeV}) \qquad (1)$$

is used. The high-energy proton escapes implosions with $\rho R \lesssim 300$ mg/cm^2. This limit is set by the charged-particle stopping power in plasmas [20]. During an implosion, a strong shock wave runs ahead of the imploding shell and rebounds at the origin several hundred ps before the main compression phase[21], creating densities

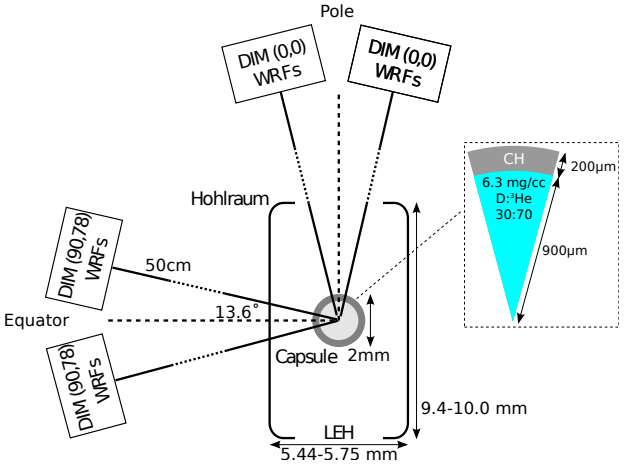

FIG. 1. WRF proton spectrometer setup for measurements of the D^3He-p spectrum in different directions at the NIF. Polar and equatorial WRFs have the same distance (50cm) and displacement from the DIM axis ($\pm 13.6^\circ$). Typical capsule dimensions shown at right.

and temperatures high enough for a brief period of fusion burn (shock bang)[22, 23] that produces protons via Eq. 1.

For the implosions[13, 24] studied at the NIF, surrogate[25] CH capsules filled with D_2 and ^{3}He gas converge to $R \sim 200 - 300\mu$m by the shock bang time (compared to an initial inner radius of $\sim 900\mu$m), at which point the total areal density has reached $\rho R \sim 60 - 120$ mg/cm^2. During the main compression burn, ρR $\gg 300$ mg/cm^2, so the D^3He-p are ranged out.

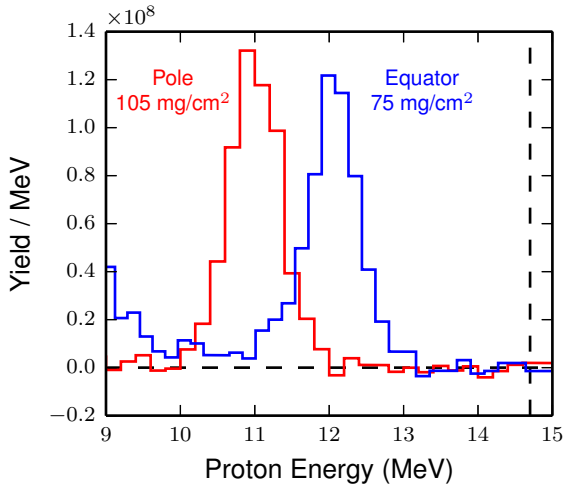

FIG. 2. Sample WRF proton spectra from NIF shot N101218 on the pole (red) and equator (blue, after hohlraum correction). The D^3He-p birth energy of 14.7 MeV is also shown (vertical dashed line). From the downshift of the measured spectra, ρR values of $105 \pm 2_{ran} \pm 6_{sys}$ mg/cm^2 (pole) and $75 \pm 2_{ran} \pm 6_{sys}$ mg/cm^2 (equator) were inferred.

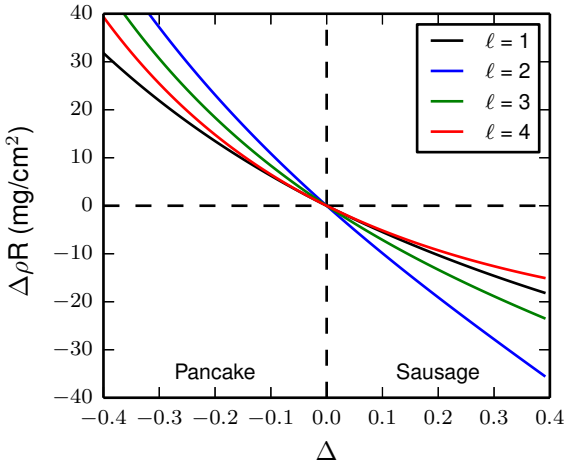

FIG. 3. Observable ρR asymmetry (pole − equator) versus mode perturbation amplitude Δ for $m = 0$ modes with $\ell = 1, 2, 3, 4$ with the shell average $\bar{R} = 265\mu$m (average $\rho R = 82$ mg/cm^2) corresponding to N101218. For a given perturbation Δ, a $\ell = 2$ mode (blue curve) causes the largest observable asymmetry.

The protons are measured with compact Wedge Range Filter (WRF) spectrometers[26–28]. Multiple spectrometers are fielded in the (0,0) polar Diagnostic Instrument Manipulator[29] (DIM) and in an equatorial DIM, (90,78), as shown in Fig. 1. WRFs in the polar DIM view the implosion through the laser entrance hole (LEH). The equatorial WRFs measure protons through the hohlraum wall which causes additional downshift; the results are corrected for this energy loss in the wall using cold-matter stopping powers[30] and known material thicknesses [31]. One or two spectrometers can be fielded at a displacement of $\pm 13.6^\circ$ from the axis for both DIMs.

In these surrogate NIF implosions, differences in the mean shock proton energy between the polar and hohlraum-corrected equatorial spectra are routinely observed. As an example, Fig. 2 shows spectra measured on the pole and equator for shot N101218, which had a large asymmetry induced by a known capsule offset. On this shot the polar WRF measured a lower shock proton energy, thus the polar ρR is higher: 105 mg/cm^2 versus 75 on the equator, for a difference $\Delta\rho R$ of 30 mg/cm^2.

Low-mode asymmetries can be modeled by spherical harmonic perturbations of the imploding shell's center-of-mass radius as

$$R_{\rm cm}(\theta, \phi) = \bar{R}\left[1 + \Delta \times \alpha e^{im\phi} P_\ell^m(\cos\theta)\right], \qquad (2)$$

where θ and ϕ are the polar and azimuthal angles, respectively, $\bar{R}$ is the unperturbed shell radius, Δ is the fractional asymmetry amplitude, α is the normalization factor[32] , and P_ℓ^m is an associated Legendre polynomial. This shape analysis using the radius enables direct comparison to x-ray metrics, which are typically given

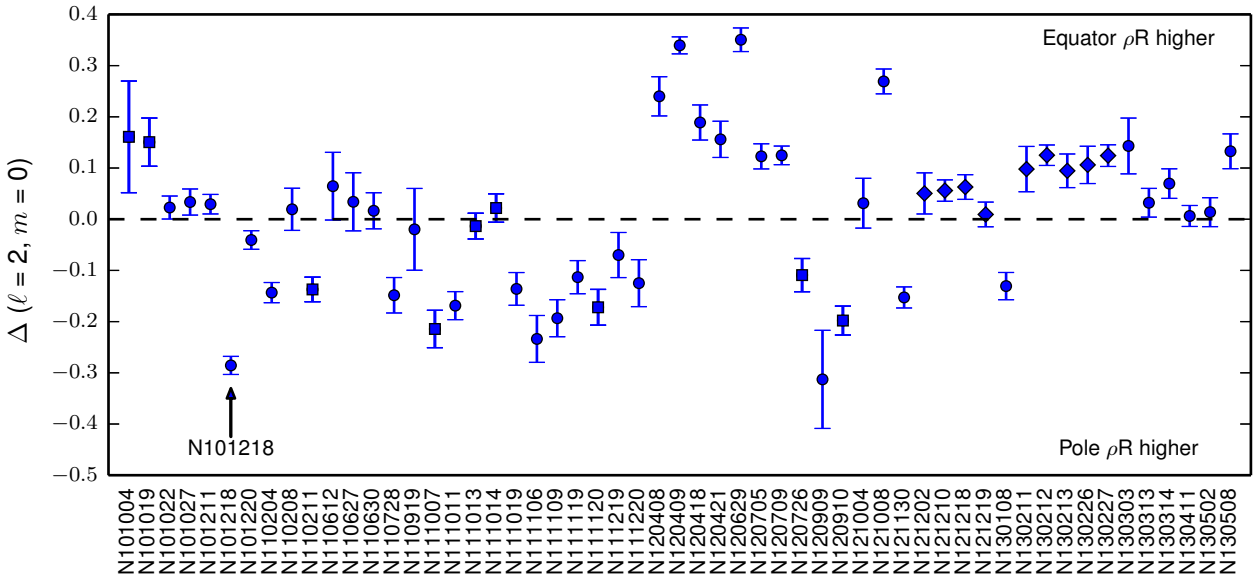

FIG. 4. Mode amplitude Δ (see Eq. 2) for all NIF shots with polar and equatorial WRF data since 2010. Shot numbers are displayed below. Displayed error bars are 1σ. Positive values represent higher ρR on the equator. Shot N101218 (also shown in Fig. 2) is specifically annotated. Shots used in Fig. 5 denoted by square markers, and in Fig 6 by diamond markers.

as fractional Legendre amplitudes (i.e. Δ). As we do not know *a priori* whether polar or azimuthal modes (or both) are responsible for observed differences between the two lines of sight (see Fig. 1), both are included here for generality.

Using a simple 1-D model, ρR and $R_{\rm cm}$ are simultaneously inferred from the proton energy measurement[33][34]. Multiple proton measurements of R_{cm} at various θ, ϕ are then fit with the functional form for $R_{\rm cm}(\theta, \phi)$ (Eq. 2)[35]. Since the asymmetries are manifested as a relative difference between the measurements, only 'random' or statistical uncertainties are retained in this analysis. The polar-equatorial geometry would suggest the assumption of a $\ell = 2, m = 0$ mode asymmetry. However, with limited WRF lines of sight we cannot differentiate between various modes. For instance, in Fig. 3 the difference in ρR between the polar and equatorial WRFs for assumed polar ($m = 0$) modes with $\ell = 1, 2, 3, 4$ are plotted. Modes 2 and 4 are known to be prevalent in these NIF implosions[8], and the potential for deleterious mode 1 asymmetries has also been recognized[36, 37].

For a given Δ, the observable difference in ρR is maximized if the mode is a P_2 (i.e. $\ell = 2, m = 0$). Fig. 3 shows that this technique is half as sensitive to modes $\ell = 1, 3, 4$ with the current detector geometry (Fig. 1). While we cannot differentiate between a $\ell = 2$ mode and a $\ell = 1$ mode with twice the perturbation amplitude, due to the limited diagnostic lines of sight (see Fig. 1)[38], for a difference in ρR between pole and equator this work assumes a $\ell = 2$ mode, which minimizes the inferred Δ. The asymmetry amplitude Δ is plotted for all shots in this work in Fig. 4, with 1σ error bars.

The ρR asymmetries do not have systematic direction, i.e. approximately the same number of shots have a higher polar ρR (negative Δ) as the number of shots with higher equator ρR (positive Δ). Only $20 - 30\%$ of the shots are consistent within error bars with a symmetric ($\Delta = 0$) implosion.

We can compare this work to compression x-ray self-

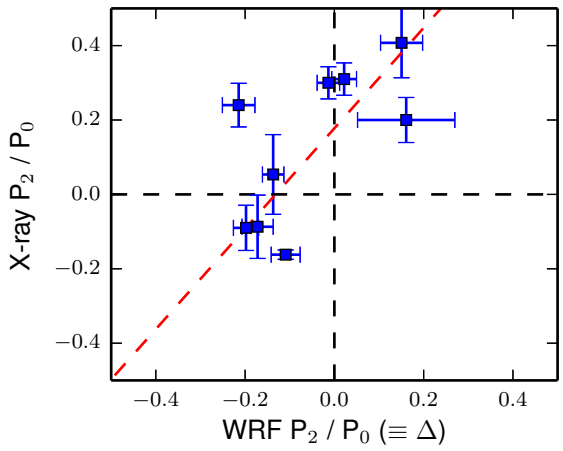

FIG. 5. Mode $\ell = 2$ amplitude from these measurements (abscissa) versus stagnation x-ray core emission shape. A linear fit (dashed red line) to the data has slope 1.35 ± 0.18 and intercept 0.21 ± 0.03. The data have a weighted Pearson correlation coefficient $p = 0.69$.

emission imaging[13, 39] at $CR \sim 20$. Restricting the dataset plotted in Fig. 4 to experiments with very good stagnation azimuthal symmetry as measured by polar-view x-ray imaging ($m_2/m_0 < 5\%$ and $m_4/m_0 < 10\%$) to reduce effects of m modes, the ρR P_2 data are compared directly to the stagnation x-ray symmetry measurement in Fig. 5. As the x-ray metric is generally referred to in literature as P_2/P_0, we follow that convention here; for the WRF measurement this is equivalent to Δ in Fig. 4.

In the data we see a correlation between the $\ell = 2$ mode amplitude inferred from the shock ρR and the stagnation x-ray emission shape. A linear fit to the data provides a slope of 1.35 ± 0.18.

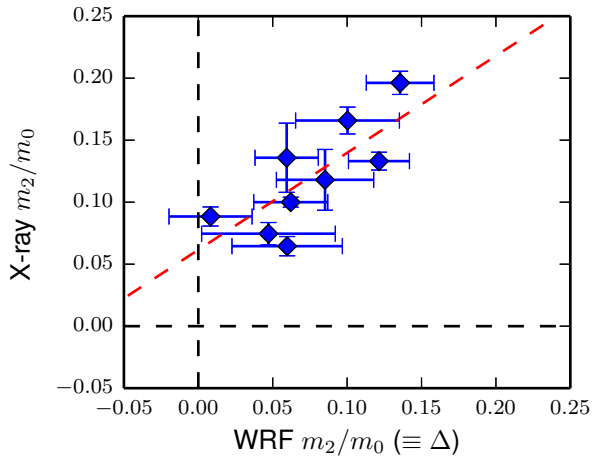

FIG. 6. Azimuthal mode amplitude inferred for experiments with in-flight x-ray imaging: this work (abscissa) versus stagnation x-ray core shape. A linear fit (dashed red line) to the data has slope 0.78 ± 0.24 and intercept 0.06 ± 0.02. The data have a weighted Pearson correlation coefficient $p = 0.77$.

To further investigate this, we use recently-developed in-flight x-ray radiography of the imploding shell, which measures the shape at a similar time in the implosion as the ρR measurements[8]. These shots correspond to a subset of Fig. 4 denoted by diamond markers. The radiography shows significant $\ell = 2$ and $\ell = 4$ modes. The radiography requires large oppositely-placed patches on the hohlraum wall, which induce a $m = 2$ asymmetry roughly aligned with the equatorial WRF line of sight. With limited lines of sight, this generates an unconstrained problem for this technique. However, if we use the radiography-measured amplitudes for $\ell = 2$ and $\ell = 4$ modes at $CR \sim 4$ and superimpose an azimuthal mode $\Delta \sin(\theta)\cos(m\phi + \phi_0)$ with $m = 2$, ϕ_0 aligned with the WRF equatorial view, and Δ a free parameter, the in-flight azimuthal shape is then characterized.

The results of this analysis are shown in Fig. 6, compared to the stagnation x-ray emission shape as in Fig. 5. Again positive correlation is observed with a slope of approximately unity: in this case 0.78 ± 0.24.

In both data sets (Figs. 5 and 6), the slope being ~ 1 indicates a lack of growth in apparent mode amplitude between shock ($CR \sim 4$) and compression ($CR \sim 20$) phases. To explore this further we consider several models for asymmetry growth of a radial $\ell = 2$ perturbation. The simplest is Bell-Plesset, a model for for asymmetric incompressible flows in spherical compression[40], which predicts a simple convergence scaling $\Delta \propto (CR - 1)$. For ICF, modified Bell-Plesset theory for compressible flows[41] is more appropriate. Finally, we also consider typical 2-D radiation hydrodynamics simulations of asymmetrically driven surrogate implosions using HYDRA[42]. The expected growth factors between the shock and compression times using these models are summarized in Table I.

TABLE I. Growth factors from shock to compression for several models.

Model	**Growth**
Bell-Plesset	$\sim 5\times$
Compressible Bell-Plesset	$\sim 3\times$
2-D HYDRA (picket&trough)[a]	$\sim 14\times$
2-D HYDRA (peak)[b]	$\sim 3\times$

[a] 10% flux asymmetry applied during the first picket and trough
[b] 10% flux asymmetry applied during the peak power

The growth factor corresponds directly to an expected slope in Figs. 5 and 6, clearly inconsistent with the data for all models. This is in contrast to previous experiments showing that the Bell-Plesset model holds for direct-drive OMEGA implosions[17, 18].

The most plausible explanation for this result is that the stagnation x-ray emission shape asymmetries do not represent (i.e. are smaller than) the ρR asymmetries at that time. A lack of correspondence between stagnation x-ray and ρR asymmetries has been seen in recent computational studies[11, 43–46], in indirect-drive OMEGA experiments[47], and in the 2-D HYDRA simulations used for Table I. This interpretation is consistent with the results of DT-layered cryogenic implosions at NIF, where neutron metrics[48–50] show very large ρR asymmetries, of order $2 - 3\times$ variation between lines of sight at compression, while the x-ray core shape is much closer to symmetric[51].

Another consideration is scenarios which cause ρR asymmetries but not shape asymmetries, such as variations in shell remaining mass or density. These scenarios would still cause significant performance degradation, and will be investigated using in-flight x-ray radiography[8] to complement this technique. Finally, the presence of $\ell = 1$ modes could affect the shock ρR but not be apparent in x-ray stagnation imaging; however we note that the asymmetry magnitudes in this work are consistent with in-flight x-ray radiography[8], suggesting

that $\ell = 1$ is not dominant. This could be verified with dedicated shots inducing $\ell = 1$ modes in these implosions, similar to recent experiments with DT fuel[36, 37].

In conclusion, compact WRF proton spectrometers fielded at the pole and equator show clear observations of implosion ρR asymmetries at the shock-bang time in D^3He surrogate experiments at the NIF. This technique is unique because it uses charged particles to probe ρR asymmetries at the shock bang several hundred ps before implosion stagnation, corresponding to a convergence ratio of $\sim 3-5$ and occurring just before peak implosion velocity, thus isolating acceleration-phase asymmetry growth. Assuming a $\ell = 2$ (P_2) mode, the data routinely show asymmetries of $\gtrsim 10\%$ at this time. These asymmetries would degrade performance later in time during stagnation, with growth factors $\gtrsim 3\times$ predicted by several models. When comparing this work to x-ray stagnation emission shape a lack of growth is observed in apparent asymmetry mode amplitude, in contrast to the expected $\gtrsim 3\times$ growth. This suggests the x-ray stagnation emission shape does not accurately reflect the stagnation shell (ρR) shape. If the asymmetries observed in this work grow as expected, the implosion performance will be degraded. Importantly, with several techniques now available for measuring the symmetry over the entire implosion evolution from $CR = 1 \rightarrow 20$, these observed asymmetries can be studied and mitigated, as necessary for ignition on the NIF.

We thank the operations crews and engineering staff at NIF for supporting these experiments, and M. McKernan, M. Cairel, and M. Valadez for their work processing the CR-39.

This work is part of the first author's Ph.D. thesis, and was supported in part by the U.S. DoE (Grant No. DE-NA0001857, DE-FC52-08NA28752), LLNL (No. B597367), LLE (No. 415935- G), the Fusion Science Center at the University of Rochester (No. 524431), and the National Laser Users Facility (No. DE-NA0002035). This material is based upon work supported by the National Science Foundation Graduate Research Fellowship Program under Grant No. 1122374.

* zylstra@mit.edu

[1] J. Nuckolls, L. Wood, A. Thiessen, and G. Zimmerman, Nature **239**, 139 (1972).
[2] J. Lindl, Phys. Plasmas **2**, 3933 (1995).
[3] G. Miller, E. Moses, and C. Wuest, Nuclear Fusion **44**, S228 (2004).
[4] S. Atzeni, EPL (Europhysics Letters) **11**, 639 (1990).
[5] S. W. Haan *et al.*, Phys. Plasmas **18**, 051001 (2011).
[6] S. Glenzer *et al.*, Science **327**, 1228 (2010).
[7] O. Landen *et al.*, Phys. Plasmas **17**, 056301 (2010).
[8] J. R. Rygg *et al.*, submitted to Phys. Rev. Lett. (2013).
[9] E. L. Dewald, J. Milovich, C. Thomas, J. Kline, C. Sorce, S. Glenn, and O. L. Landen, Phys. Plasmas **18**, 092703 (2011).
[10] E. L. Dewald *et al.*, Phys. Rev. Lett. **111**, 235001 (2013).
[11] R. Town *et al.*, submitted to Phys. of Plasmas (2013).
[12] J. Moody *et al.*, submitted to Phys. of Plasmas (2013).
[13] G. Kyrala *et al.*, Rev. of Sci. Instrum. **81**, 10E316 (2010).
[14] S. H. Glenzer *et al.*, Plasma Physics and Controlled Fusion **54**, 045013 (2012).
[15] G. P. Grim *et al.*, Phys. Plasmas **20**, 056320 (2013).
[16] T. Boehly *et al.*, Optics Communications **133**, 495 (1997).
[17] J. A. Frenje *et al.*, Phys. Plasmas **11**, 2798 (2004).
[18] C. K. Li *et al.*, Phys. Rev. Lett. **92**, 205001 (2004).
[19] R. Petrasso *et al.*, Phys. Rev. Lett. **90**, 095002 (2003).
[20] C. Li and R. Petrasso, Phys. Rev. Lett. **70**, 3059 (1993).
[21] Relative bang times will be measured precisely in the future[52].
[22] G. Guderley, Luftfahrtforsch **19**, 302 (1942).
[23] J. R. Rygg, (Massachusetts Institute of Technology, 2006).
[24] D. G. Hicks, B. K. Spears, D. G. Braun, R. E. Olson, C. M. Sorce, P. M. Celliers, G. W. Collins, and O. L. Landen, Phys. Plasmas **17**, 102703 (2010).
[25] The cryogenic DT ice layer of an ignition target is replaced with an equivalent mass of ablator material. The implosion dynamics are equivalent until deceleration and stagnation.
[26] F. Séguin *et al.*, Rev. Sci. Instrum. **74**, 975 (2003).
[27] F. H. Seguin *et al.*, Rev. Sci. Instrum. **83**, 10D908 (2012).
[28] A. B. Zylstra *et al.*, Rev. Sci. Instrum. **83**, 10D901 (2012).
[29] W. J. Hibbard, M. D. Landon, M. D. Vergino, F. D. Lee, and J. A. Chael, Rev. Sci. Instrum. **72**, 530 (2001).
[30] J. Ziegler, J. Biersack, and U. Littmark, (Pergamon, New York, 1985).
[31] Total correction is $\sim 1.5-2$ MeV. Uncertainty in the material thickness leads to an additional error of $\pm$ 50 to 75 keV in the total energy uncertainty.
[32] Such that the spherical harmonics are normalized, $\alpha = \sqrt{\frac{2\ell+1}{4\pi}\frac{(\ell-m)!}{(\ell+m)!}}$.
[33] A. B. Zylstra *et al.*, to be submitted to Phys. of Plasmas (2014).
[34] A mass profile is self-consistently converged to relate R_{cm}, ρR, and measured proton energy. From the measured proton energy, R_{cm} and ρR are then inferred.
[35] For the low modes considered, the variations are much larger than the detector solid angle ($\sim 1^\circ$ subtended) so using a local value of $R_{cm}(\theta, \phi)$ and thus $\rho R(\theta, \phi)$ is a good approximation.
[36] J. Kilkenny *et al.*, submitted to EPJ Conf. Series (2013).
[37] B. Spears *et al.*, Submitted to Phys. Plasmas (2013).
[38] By fielding additional WRFs in key locations around the implosion the in-flight shape could be further constrained, for example at $\theta = 45^\circ$ to measure $\ell = 4$ modes; near the south pole at $\theta \sim 180^\circ$ to measure $\ell = 1$, and at multiple locations around the equator to constrain m modes.
[39] D. K. Bradley, P. M. Bell, J. D. Kilkenny, R. Hanks, O. Landen, P. A. Jaanimagi, P. W. McKenty, and C. P. Verdon, Rev. of Sci. Instrum. **63**, 4813 (1992).
[40] M. S. Plesset, Journal of Applied Physics **25**, 96 (1954).
[41] P. Amendt, J. D. Colvin, J. D. Ramshaw, H. F. Robey, and O. L. Landen, Phys. Plasmas **10**, 820 (2003).
[42] M. Marinak, G. Kerbel, N. Gentile, O. Jones, D. Munro, S. Pollaine, T. Dittrich, and S. Haan, Phys. Plasmas **8**,

2275 (2001).
[43] R. H. H. Scott *et al.*, Phys. Rev. Lett. **110**, 075001 (2013).
[44] A. Kritcher *et al.*, APS DPP Bulletin , NO4.00004 (2013).
[45] J. Gu, Z. Dai, Z. Fan, S. Zou, W. Ye, W. Pei, and S. Zhu, Phys. Plasmas **21**, 012704 (2014).
[46] A. Kritcher *et al.*, submitted to Phys. of Plasmas (2014).
[47] N. Izumi *et al.*, APS DPP Bulletin , BO1.010 (2004).
[48] D. L. Bleuel *et al.*, Rev. of Sci. Instrum. **83**, 10D313 (2012).
[49] C. B. Yeamans, D. L. Bleuel, and L. A. Bernstein, Rev. of Sci. Instrum. **83**, 10D315 (2012).
[50] J. Frenje *et al.*, Nuclear Fusion **53**, 043014 (2013).
[51] M. J. Edwards *et al.*, Phys. Plasmas **20**, 070501 (2013).
[52] H. G. Rinderknecht *et al.*, Rev. Sci. Instrum. **83**, 10D902 (2012).